Hybrid noise control in a duct using a light micro-perforated plate

X. N. Wang, Y. S. Choy, and L. Cheng[a]

Department of Mechanical Engineering, The Hong Kong Polytechnic University, Hung Hom, Kowloon, Hong Kong Special Administrative Region, China

A plate silencer consists of an expansion chamber with two side-branch cavities covered by light but extremely stiff plates. It works effectively with a wide stopband from low-to-medium frequencies only if the plate is extremely stiff, to ensure a strong reflection of acoustic wave to the upstream in the duct. However, a plate with a slightly weak bending stiffness will result in non-uniform transmission loss (TL) spectra with narrowed stopband. In this study, a hybrid silencer is proposed by introducing micro-perforations into the plate to elicit the sound absorption in order to compensate for the deficiency in the passband caused by the insufficient sound reflection in a certain frequency range due to weaker plate stiffness. A theoretical model, capable of dealing with the strong coupling between the vibrating micro-perforated plate and sound fields inside the cavity and the duct, is developed. Through proper balancing between the sound absorption and reflection, the proposed hybrid silencer provides a more flattened and uniform TL and a widened stopband by more than 20% while relaxing the harsh requirement on the bending stiffness of the plate. Theoretical predictions are validated by experimental data, with phenomenon explained through numerical analyses. © *2012 Acoustical Society of America*. [http://dx.doi.org/10.1121/1.4763550]

PACS number(s): 43.50.Gf, 43.55.Ev [NX]   Pages: 3778–3787

I. INTRODUCTION

Abatement of low frequency noise has always been a challenging topic. Most traditional methods such as porous duct lining and expansion chamber still suffer from serious drawbacks. Despite its wide use in air conditioning and ventilation systems, duct lining with a porous sound absorbing material fails to perform well at low frequencies because of its high characteristic impedance. Meanwhile fibrous materials cause the environmental concerns such as accumulation of dusts in the pores of the porous material and bacteria breeding. Expansion chambers usually occupy a relatively large volume in order to cope with low frequency noise, at the expense of creating significant pressure loss in a flow duct, and loosing efficiency at multiple frequencies at which the chamber length equals half a wavelength.

Aiming at a compact, broadband, and relatively low frequency noise control device, a continuous effort has been made to develop silencers comprising an expansion chamber with two side-branch cavities covered with plates.[1,2] The working principle of such a device, referred to as a plate silencer, makes use of a sound reflection mechanism inside a duct. Upon proper tuning of the plate parameters, the plate, flush-mounted with the inner duct wall, reflects the sound to the upstream side, creating favorable interference with the incoming sound. While the promises of this new technique were well demonstrated in our previous work, there still exist some serious limitations hampering its application, which are mainly twofold: (1) The plate should have a very high

bending stiffness and a very low mass ratio. For example, to ensure a reasonable level of structural response induced by an acoustic incident wave, the mass ratio of plate to air should be about unity. Meanwhile the dimensionless bending stiffness should be about 0.07, which is equivalent to an aluminum plate 1.4 mm thick with the same width. However, a 1.4 mm thick aluminum plate has a mass ratio to air of approximately 25.3, which far exceeds the desirable mass ratio range. Therefore, a plate silencer purely based on sound reflection puts a very harsh requirement which can hardly be satisfied by conventional materials, not even the specially designed sandwich plates[2] or the carbon fiber (CF) reinforced composite plates[3] in the most rigorous sense. Failing to do so results in a significant reduction in both the transmission loss (TL) level and the stopband. (2) The performance of the silencer is highly non-uniform across the frequency range, as demonstrated by the drastic fluctuation as well as the existence of troughs (passband) in the medium frequency range of the TL curve. This not only directly contributes to narrowing the stopband of the device but also limits the use of the device for broadband noise control.

In order to achieve a wider stopband, a hybrid silencer is proposed in this work by introducing micro-perforations into a very light and moderately stiff plate. The purpose of the micro-perforations is to add sound absorptions to compensate for the deficiency in the passband caused by the insufficient sound reflection due to the plate with a weaker strength to mass ratio. The proposed hybrid silencer differs from the existing plate silencer in that sound reflection and absorption take a dominant effect at different frequency ranges to provide a more flattened/uniformed TL curve. That is the reason why this silencer is referred to as "hybrid." By the same token, the harsh requirement in terms of high

[a]Author to whom correspondence should be addressed. Electronic mail: mmlcheng@polyu.edu.hk

bending stiffness is relaxed along with an enlargement of the stopband, as will be shown later in the paper. The proposed hybrid silencer also differs from the traditional micro-perforated plate (MPP) absorber design, which is proposed by Maa[4] and extensively used in the different areas such as room acoustics,[5–7] barrier design,[8] and duct.[9–12] A typical MPP absorber takes the form of an MPP in front of a backing cavity that can achieve Helmholtz sound absorption.[13–15] In the past, the use of a micro-perforated tube or plate in a single expansion chamber[9,10] or multiple chamber[11] was also investigated, entirely for sound absorption with an acoustically rigid micro-perforated structure. Up to now, most existing studies in such studies focused on the function of the MPP device itself without considering the vibration of the plate and its vibroacoustic coupling with the sound field in the duct.

The proposed hybrid silencer consists of two light and moderately stiff plates with micro-perforations, covering two rectangular cavities. With the grazing in-coming waves passing over the surface of the plate, the plate is excited to vibrate, which in turn radiates sound both upstream and downstream. Meanwhile, the radiated sound pressure in both the duct and inside the cavity interacts with the plate vibration, forming a strongly coupled vibroacoustic system. With the micro-perforations, part of the acoustic energy is absorbed and by the same token, the response of the plate, as well as its sound radiation, is expected to be affected. The balance between the compromised sound reflection and enhanced sound absorption is the key to achieve a flattened and widened stopband in the TL curve, conducive to broadband noise control.

The objectives of this study are (1) to establish a theoretical vibroacoustic model, which takes into account the full coupling between the MPP and the sound field in a duct and cavity; (2) to understand the underlying physics related to the sound reflection and absorption due to the use of micro-perforation as well as its impact on the silencer performance; and (3) to propose guidelines toward the optimal design of an effective hybrid silencer.

In what follows, Sec. II outlines the theoretical model for the plate silencer with micro-perforations. Modal expansion is used to solve the fully coupled system among the plate, the cavity, the duct and the micro-perforated orifices. A performance analysis will be carried out in Sec. III. The response of the plate, interaction between sound absorption, and sound radiation from the plate will be analyzed. An optimization process is to be conducted in order to search for optimal physical parameters such as properties of perforations and structural properties of the plate so that the best performance can be obtained. An experimental validation will be given in Sec. IV.

II. FORMULATION

A two-dimensional model of a side-branch plate silencer is shown in Fig. 1. The geometry resembles a standard expansion chamber with a main duct having a height of h^*, two identical rectangular cavities of length L^* and depth h_c^*. The asterisks denote the dimensional variables while the corresponding dimensionless ones are introduced shortly without asterisks. Two micro-perforated plates are used to cover the cavities. A plane incident sound wave is assumed to come from left to right with unit amplitude

$$p_i^* = e^{i(\omega^* t^* - k_0^* x^*)}, \tag{1}$$

and it excites the plate into vibration with a transverse displacement of complex amplitude η_p^* and velocity v_p^* with the same time dependence, $e^{i(\omega^* t^*)}$. The plate motion radiates sound in both directions of the duct and also induces a fluid loading on itself from both the cavity and the duct side. The plate vibration is governed by the following equation:

$$B^* \frac{\partial \eta_p^*}{\partial (x^*)^4} + m^* \frac{\partial^2 \eta_p^*}{\partial (t^*)^2} + (p_i^* + p_{\text{duct}}^* - p_{\text{cav}}^*) = 0, \tag{2}$$

where B^* is the bending stiffness of the plate, m^* is the plate mass per unit surface area, and p_{duct}^* and p_{cav}^* is the radiation pressure in the duct and cavity, respectively.

Now consider the micro-perforation, which is a lattice of sub-millimeter holes uniformly distributed over the surface of the plate: The sound pressure difference applied between two sides of the plate generates the air mass vibration in the holes. As the orifice diameter is much smaller than the acoustic wavelength of interest, the air particle velocity is assumed to be distributed uniformly within the area of each hole and the air solid interaction is given by[16]

$$Z_{\text{resist},0}(v_0^* - v_p^*) + Z_{\text{react},0} v_0^* + \frac{1}{\rho_0^* c_0^*}(p_i^* + p_{\text{duct}}^* - p_{\text{cav}}^*) = 0, \tag{3}$$

where v_0^* is the particle velocity in one single hole and v_p^* is the vibration velocity of the plate. Z_0 denotes the complex
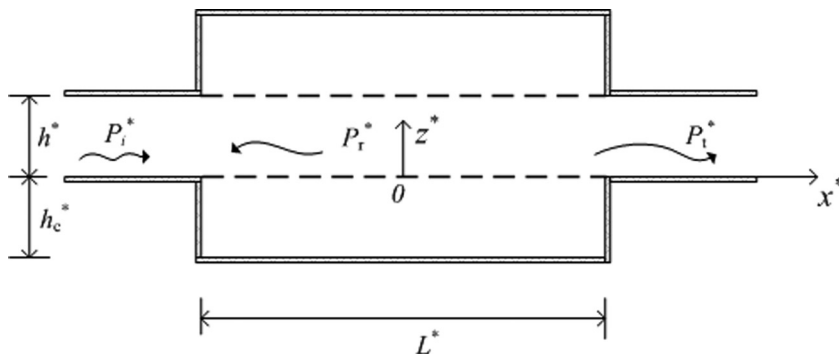
FIG. 1. Theoretical model for the plate silencer in a rectangular cavity using two plates with micro-perforation.

J. Acoust. Soc. Am., Vol. 132, No. 6, December 2012

Wang *et al.*: Hybrid silencer in a duct   3779

acoustic impedance of the hole normalized by the characteristic impedance of the air $\rho_0^* c_0^*$. $Z_{\text{resist},0}$ and $Z_{\text{react},0}$ are the resistant and reactant parts of Z_0, respectively, which are proposed by Maa,[4]

$$Z_0 = Z_{\text{resist},0} + Z_{\text{react},0}$$
$$= \frac{32\mu^*\tau^*}{\rho_0^* c_0^* (d^*)^2}\left[\left(1 + \frac{K^2}{32}\right)^{0.5} + \frac{\sqrt{2}Kd^*}{32\tau^*}\right]$$
$$+ \frac{i\omega^*\tau^*}{c_0^*}\left[1 + \left(1 + \frac{K^2}{32}\right)^{-0.5} + 0.85\frac{d^*}{\tau^*}\right], \quad (4)$$

where τ^* is the thickness of the plate, d^* is the diameter of the hole, μ^* is the coefficient of viscosity, and $K = d^*/2\sqrt{\rho_0^*\omega^*/\mu^*}$.

All the dimensional variables used are nondimensionalized by three quantities: Air density ρ_0^*, speed of sound in free space c_0^*, and duct height h^* as

$$x = \frac{x^*}{h^*}, \quad z = \frac{z^*}{h^*}, \quad h_c = \frac{h_c^*}{h^*}, \quad L = \frac{L^*}{h^*}, \quad \eta_p = \frac{\eta_p^*}{h^*},$$
$$f = \frac{f^* h^*}{c_0^*}, \quad m = \frac{m^*}{\rho_0^* h^*}, \quad B = \frac{B^*}{\rho_0^* (h^*)^3 (c_0^*)^2},$$
$$p = \frac{p^*}{\rho_0^* (c_0^*)^2}, \quad d = \frac{d^*}{h^*}, \quad \tau = \frac{\tau^*}{h^*}, \quad \mu = \frac{\mu^*}{\rho_0^* c_0^* h^*}. \quad (5)$$

Assuming the plate is in harmonic motion $v_p = \partial\eta_p/\partial t = i\omega\eta_p$, Eq. (2) can be written as

$$\frac{B}{i\omega}\frac{\partial^4 v_p}{\partial x^4} + mi\omega v_p + (p_i + p_{\text{duct}} - p_{\text{cav}}) = 0. \quad (6)$$

Equation (3) turns into

$$Z_{\text{resist},0}(v_0 - v_p) + Z_{\text{react},0}v_0 + p_i + p_{\text{duct}} - p_{\text{cav}} = 0. \quad (7)$$

An average air velocity $\bar{v}_0$ is obtained by averaging the discrete air particle velocity over each orifice across the adjacent imperforated region of the plate as

$$\bar{v}_0 = v_0\sigma, \quad (8)$$

where σ is the perforation ratio of the plate. The dynamics of the plate described in Eqs. (6) and (7) can be solved by the standard Galerkin procedure in which $v_p(x)$ is expanded as a series of *in vacuo* modes $\varphi_j(\xi)$ of the clamped-clamped plates with modal amplitude $V_{p,j}$

$$v_p(x) = \sum_{j=1}^{\infty} V_{p,j}\varphi_j(\xi), \quad \xi = x/L + 1/2, \quad (9)$$

where

$$\varphi_j(\xi) = A_{1,j}e^{\lambda_j\xi} + A_{2,j}e^{-\lambda_j\xi} + A_{3,j}\sin(\lambda_j\xi)$$
$$+ A_{4,j}\cos(\lambda_j\xi), \quad (10)$$

with

$$A_{1,j} = \frac{1}{2}(1 - \varepsilon_j), \quad A_{2,j} = \frac{1}{2}(1 + \varepsilon_j), \quad A_{3,j} = \varepsilon_j, \quad A_{4,j} = -1,$$
$$(11)$$

$$\varepsilon_j = \frac{\cosh(\lambda_j) - \cos(\lambda_j)}{\sinh(\lambda_j) - \sin(\lambda_j)}, \quad \cos(\lambda_j) \cdot \cosh(\lambda_j) = 1. \quad (12)$$

So $\bar{v}_0$ is also expanded over the same series $\varphi_j(\xi)$ as

$$\bar{v}_0(x) = \sum_{j=1}^{\infty} \bar{V}_{0,j}\varphi_j(\xi). \quad (13)$$

So $v_0(x) = \sum_{j=1}^{\infty} V_{0,j}\varphi_j(\xi)$ with $V_{0,j} = \bar{V}_{0,j}/\sigma$.

Therefore, Eqs. (6) and (7) become

$$\left\{\frac{B}{i\omega}\left(\frac{\beta_j}{L}\right)^4 + mi\omega\right\}V_{p,j} + \int_0^1 (p_i + p_{\text{duct}} - p_{\text{cav}})\varphi_j(\xi)d\xi = 0, \quad (14)$$

$$Z_{\text{resist},0}(V_{0,j} - V_{p,j}) + Z_{\text{react},0}V_{0,j}$$
$$+ \int_0^1 (p_i + p_{\text{duct}} - p_{\text{cav}})\varphi_j(\xi)d\xi = 0, \quad (15)$$

respectively.

Given the average velocity distribution for the whole plate with micro-perforations, $\bar{v}(x)$, which is defined as $\bar{v}(x) = (1 - \sigma)v_p(x) + \bar{v}_0(x)$, the radiated pressure p_{duct} can be calculated as[17]

$$p_{\text{duct}}(x, z) = \frac{L}{2}\sum_{n=0}^{\infty} c_n\phi_n(z)$$
$$\times \int_0^1 \bar{v}(x')\phi_n(z')[H(x - x')e^{-ik_n(x-x')}$$
$$+ H(x' - x)e^{+ik_n(x-x')}]d\xi', \quad (16)$$

with

$$c_n = \frac{i}{\sqrt{(n\pi/\omega)^2 - 1}}, \quad k_n = \frac{\omega}{c_n},$$
$$\phi_n(z) = \sqrt{2 - \delta_{0n}}\cos(n\pi z), \quad (17)$$

where $H(x)$ is the Heaviside function, δ_{0n} is the Kronecker delta, c_n, k_n, ϕ_n are, respectively, modal phase speed, modal wave number, and the modal velocity potential. The source is specified as a plate vibration at $z' = 0$, $x' \in [-L/2, L/2]$.

Assuming that the radiation pressure caused by the jth modal vibration of unit amplitude φ_j is $p_{\text{duct},j}$, the duct modal impedance is then defined as

$$Z_{\text{duct},jl} = \int_0^1 p_{\text{duct},j}(x, 0)\varphi_l(\xi)d\xi. \quad (18)$$

The sound pressure inside the cavity p_{cav}, can be expressed in terms of acoustic modes of rigid-walled cavity with a light damping[18]

$$p_{\text{cav}}(x, z) = \sum_{r,s} \frac{-i\omega\psi_{rs}(x, z)}{Lh_c(\kappa_{rs}^2 - k_0^2 + 2i\zeta_{rs}\kappa_{rs}k_0)}$$
$$\times \int_0^1 \bar{v}(x', 0)\psi_{rs}(x', 0)d\xi', \quad (19)$$

where ζ_{rs} is the damping ratio of the (r,s)th acoustic mode $\psi_{rs}(x,z)$, and κ_{rs} is the corresponding acoustic wave number of the acoustic mode $\psi_{rs}(x,z)$, with $\psi_{rs}(x,z)$ and κ_{rs} given as

$$\psi_{rs}(x,z) = \sqrt{(2-\delta_{0r})(2-\delta_{0s})} \cos\left(\frac{r\pi x}{L}\right)\cos\left(\frac{s\pi z}{h_c}\right),$$
(20)

$$\kappa_{rs}^2 = \left(\frac{r\pi}{L}\right)^2 + \left(\frac{s\pi}{h_c}\right)^2.$$
(21)

Similarly, the cavity modal impedance is given as

$$Z_{\text{cav},jl} = -\int_0^1 p_{\text{cav},j}(x,0)\varphi_l(\xi)d\xi.$$
(22)

Therefore, Eqs. (14) and (15) can be cast into a set of linear equations in terms of modal vibration in j mode as

$$L_j V_{p,j} + (Z_{\text{duct},jl} - Z_{\text{cav},jl})[(1-\sigma)V_{p,j} + \sigma V_{0,j}] = -I_j,$$
(23)

$$Z_{\text{resist},0}(V_{0,j} - V_{p,j}) + Z_{\text{react},0}V_{0,j}$$
$$+ (Z_{\text{duct},jl} - Z_{\text{cav},jl})[(1-\sigma)V_{p,j} + \sigma V_{0,j}] = -I_j, \quad (24)$$

where $L_j = \{(B/i\omega)(\beta_j/L)^4 + mi\omega\}$, and I_j is the modal coefficient of incident waves which is defined as

$$I_j = \int_0^1 p_i \varphi_j(\xi)d\xi.$$
(25)

$V_{0,j}$ and $V_{p,j}$ can be solved through matrix inversion.

The total sound pressure transmitted to the downstream is found by adding the incident wave p_i to the far-field radiation wave p_{duct}, which can be found with the help of Eq. (16) by taking only the plane wave mode with $n = 0$ for $x > L/2$

$$p_t = p_{\text{duct}}|_{n=0,x\to+\infty} + p_i.$$
(26)

Similarly

$$p_r = p_{\text{duct}}|_{n=0,x\to-\infty}.$$
(27)

Hence, for an incident wave of unit amplitude, the TL of the silencer can be calculated as

$$\text{TL} = -20\log_{10}\frac{|p_t|}{|p_i|}.$$
(28)

The coefficients of sound power reflected and absorbed are calculated, respectively, by

$$\beta = \left|\frac{p_r}{p_i}\right|^2, \quad \alpha = 1 - \beta - \left|\frac{p_t}{p_i}\right|^2,$$
(29)

where p_r is given by

$$p_r = \frac{1}{2}\int_{-L/2}^{L/2} \bar{v}(x')e^{-ik_0x'}dx' = \sum_{j=1}^{\infty} \bar{V}_j R_j,$$
(30)

with

$$R_j = \int_{-L/2}^{L/2} \varphi_j(\xi')e^{-ik_0x'}dx'.$$
(31)

R_j is the complex amplitude of the reflected sound by the induced vibration of the jth mode with unit amplitude, and $\bar{V}_j R_j$ is defined as the modal reflection which evaluates the reflection ability for each mode.

III. NUMERICAL RESULTS AND ANALYSES

A plate silencer with micro-perforations involves many variables. A performance study is first carried out with most variables fixed such that the length of the plate ($L = 5$), the cavity depth ($h_c = 1$), the height of the duct ($h = 1$), and the mass ratio of the plate ($m = 1$). The bending stiffness of the plate is a very influential parameter which is varied while studying the effect of the micro-perforation properties such as the diameter of the holes, the perforation ratio, and the thickness of the plate. The performance of the plate-silencer is evaluated by the logarithmic width of its stopband, defined as the frequency range in which TL is everywhere equal to or greater than a suitable criterion level (TL_{cr}). Expressed symbolically, $f \in [f_1,f_2]$ in which $\text{TL} \geqq \text{TL}_{\text{cr}}$ and $\text{TL}_{\text{cr}} = 10\,\text{dB}$ in the present study. A cost function is set as the ratio of the band limits f_2/f_1 in the design optimization.

In order to ensure the accuracy of the calculation, the duct, cavity, and plate modes are truncated to 50, 50, and 25, respectively. A further increase in the number of modes does not make a noticeable improvement in the calculation results within the frequency range of interest of the present work.

A. Perforation effect

The effect of the micro-perforation on the TL is first shown before detailed analyses are presented Secs. III B–III E. Figure 2 compares the TL of the plate silencer with and without micro-perforations under three configurations. The TL curve of a plate silencer without perforation with $B = 0.07$, previously determined as the optimal bending stiffness for the plate silencer without any perforations, is shown as the dotted line. Three peaks are observed, which have been shown to be caused by the strong sound reflection from the plate due to the dominance of the first two modes of the plate. The stopband begins from $f_1 = 0.044$ and ends at $f_2 = 0.124$, corresponding to $f_2/f_1 = 2.81$. Note that the bending stiffness required is very high. Reducing B by about 20% down to 0.057, the trough between the second and third peak in the TL curve drastically drops down, resulting in a TL of less than 10 dB so that the overall stopband is significantly decreased to $f_2/f_1 = 2.21$ (dashed line). Keeping the same bending stiffness at $B = 0.057$, perforations with $\sigma = 0.7\%$ and nondimensional diameter $d = 0.007$ (dimensional diameter $d^* = 0.7\,\text{mm}$), are then added to the plate. It can be seen that the micro-perforation effect can lift up the trough point between the second and third peak so that a more flattened TL curve is obtained. Meanwhile, compared to TL of $B = 0.07$, while basically keeping the same f_1, the third peak on the TL curve is moved to a higher frequency so that the stopband ends at a much higher frequency
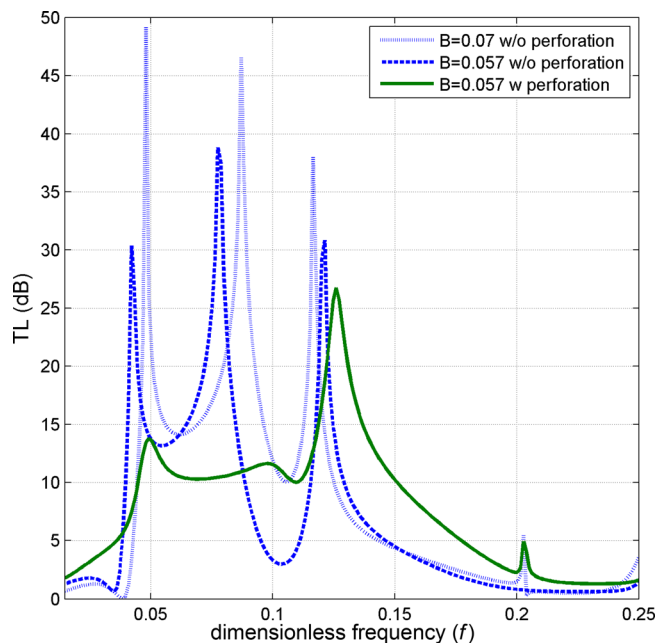
FIG. 2. (Color online) TL of the plate silencer with a different plate: The plate ($m = 1$ and $B = 0.07$) without perforation (dotted line), the plate ($m = 1$ and $B = 0.057$) without perforation (dashed line); the plate ($m = 1$ and $B = 0.057$) with micro-perforation ($\tau = 0.04$, $d = 0.007$, and $\sigma = 0.7\%$) (solid line).

FIG. 3. (Color online) Comparison between the plate with and without perforations (a) TL, (b) reflection coefficient β, and (c) absorption coefficient α.

at $f_2 = 0.15$. This corresponds to $f_2/f_1 = 3.45$, a significant broadening of the stopband by about 23% as compared to the optimally designed stiff plate silencer, or 56% as compared to the one having the same bending stiffness but without perforation. Therefore, the use of micro-perforation in the plate seems to result in a more uniform TL with a broader stopband by using a less stiff plate. This is beneficial for coping with broadband noise control. By the same token, the harsh requirement on the high bending stiffness of the plate imposed by the original silencer design is also being relaxed. Underlying physics explaining these effects are carried out in Secs. III B–III F.

B. Reflection vs absorption

Analyses are performed to explore the underlying physics to explain such improvement on the stopband due to the addition of micro-perforations on the plate. In particular, the effectiveness of sound reflection, sound absorption enhancement by the micro-perforated plate (MPP) as well as the plate response is to be discussed. Using $B = 0.057$, the reflection coefficient (β) and the absorption coefficient (α) are shown in Fig. 3, together with the corresponding TL curve to facilitate the analysis of the peak and trough frequency variation. It can be observed from Figs. 3(a) and 3(b) that, without perforation, the plate silencer purely relies on the strong sound reflection, as evidenced by the high β regions to create high TL peaks. The addition of the micro-perforation generally reduces the sound reflection from the plate. Roughly speaking, upon deployment of the micro-perforation, the whole reflection coefficient spectra seem to be slightly shifted to higher frequencies and hence an enhancement of reflection coefficient for $f > 0.13$ is
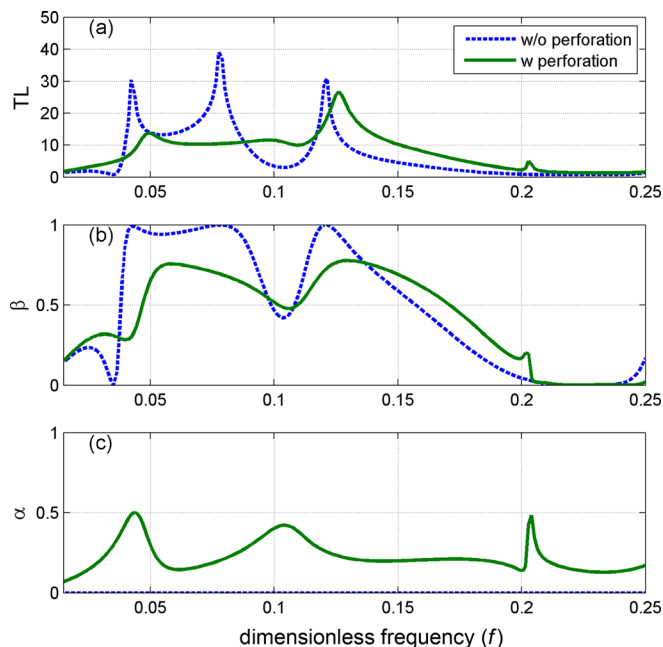
observed. Figure 3(c) shows the corresponding absorption coefficient spectrum. Without perforations, there is practically no absorption so the dashed line is keeping zero at all frequencies. With micro-perforations, the absorption coefficient is about 0.3 on average with two peaks at $f = 0.043$ and $f = 0.104$, respectively, which do not exactly coincide with peaks in TL spectra. The nature of these absorption peaks will be examined later. It is, however, pertinent to note that the second peak at $f = 0.104$, with α about 0.42, directly contributes to the increase in TL, where the original trough region without micro-perforation is elevated. So with the addition of micro-perforations, three main observations can be made: (1) All TL peaks are smoothed out while slightly shifting to higher frequencies; (2) the original trough point of TL for the plate without micro-perforation is raised up mainly because of the sound absorption; and (3) the stopband is widened due to the shift of the third dominant peak to a higher frequency.

C. TL peaks

The aforesaid phenomenon pertaining to TL peaks is investigated through analyzing the modal amplitude $|\bar{V}_j|$ and modal reflection $|\bar{V}_j R_j|$. $|\bar{V}_j|$ of the first three modes of the plate are shown in the first column of Fig. 4. The higher order modal responses are relatively weak so they are not shown here. For comparison, the modal reflections, $|\bar{V}_j R_j|$, from the same modes are shown in the second column. Three circles and three crosses marked on the curves correspond to the frequencies of three TL peaks without perforation (dashed line) and with perforation (solid line), respectively. It can be seen that in both cases (with and without perforation), the first peak of TL is attributed to the first and second modes simultaneously. The second peak of TL is mainly
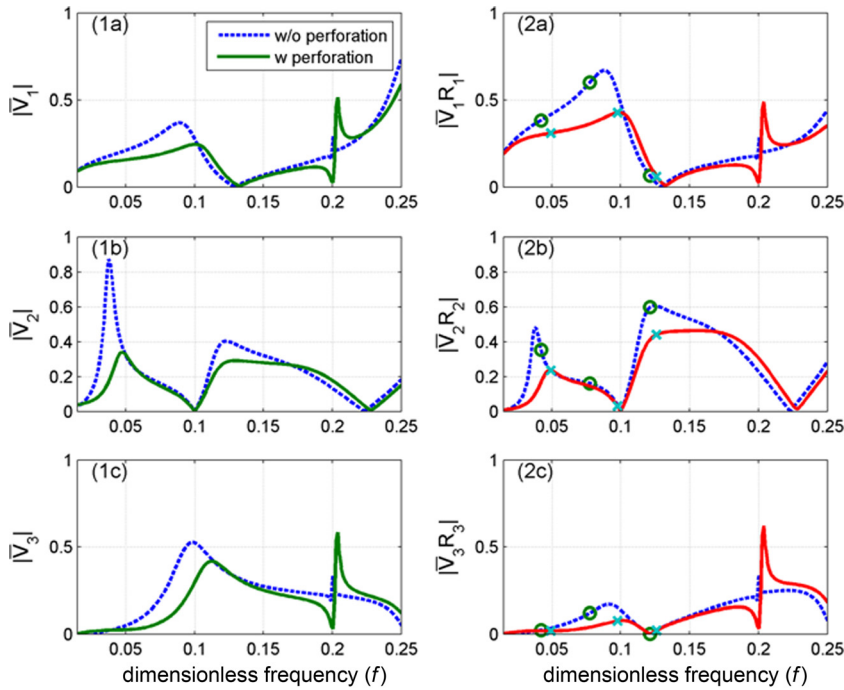
FIG. 4. (Color online) Modal analysis. The first column is the modal amplitude $|\bar{V}_j|$ and the second column is the modal reflection $|\bar{V}_j R_j|$, $j = 1,2,3$.

dominated by the first mode while the third peak of TL is due to the second modal contribution. For the micro-perforated plate, the first peak of TL is reduced as a result of a reduction in both $|\bar{V}_1|$ and $|\bar{V}_2|$, as shown in Figs. 1(a) and 1(b). This is due to the fact that the introduction of the micro-perforation brings about a certain degree of pressure balance across the perforated panel through the holes so that the resulting excitation on the plate is reduced, leading to an ultimate reduction in the response of the plate. A similar trend can also be observed from the variation of $|\bar{V}_1 R_1|$ and $|\bar{V}_2 R_2|$, shown in Figs. 4(2a) and 4(2b), respectively. Compared to the plate without micro-perforation, the sound reflection from the perforated plate is also reduced. It should be noted that the terminology "reflection" is being used loosely here to be consistent with previous work. In fact, sound is "reflected" to upstream mainly due to the radiation of the vibrating plate. In that sense, the reduced vibration response of the perforated plate due to a better pressure balance is the direct cause of the impaired sound reflection. Meanwhile, the radiation efficiency of the plate is, in principle, also impaired[19,20] due to the micro-perforation. This also contributes to the impaired sound reflection and consequently reduced TL peak values.

The phase relationship between the air vibration of the perforation and the plate vibration were checked (not shown here). It was observed that they do not always have a simple phase relationship, although they are rather in phase in a large frequency range considered. The average air velocity, $\bar{v}_0$, however, has basically always the same phase as the plate vibration. This suggests that the overall behavior of the MPP is mainly dominated by the plate vibration. The relative air motion of the perforation with respect to the plate, although critical to the sound absorption of the MPP, is not the most dominant factor in terms of

the interaction between the MPP and the surrounding acoustic media.

D. Peaks in sound absorption coefficient

The lifting of the TL trough is mainly attributed to the peak of the sound absorption coefficient in that frequency range. The hybrid silencer is a complex system involving the coupling among the duct, plate, and cavity. This can be best seen in terms of the system impedance. Figure 5 show the total reactance $(\mathrm{Im}(Z_{jl}) = \mathrm{Im}(L_j + Z_{\mathrm{duct},jl} - Z_{\mathrm{cav},jl}))$ for the first two plate modes without perforations. When the cross-modal coupling is ignored, the coupled system resonates where the total reactance vanishes. The first resonance now occurs at $f = 0.182$, which is beyond the second *in vacuo* natural frequency of the plate, from which one can see the strong coupling between the plate and the cavity due to the symmetrical nature of the first plate mode. The first and second resonance points found in Figs. 5(a) and 5(b) marked with a circle roughly correspond to the third and first peaks in the sound absorption coefficient, respectively, as shown in Fig. 3(c). On the other hand, the second peak of sound absorption coefficient at $f = 0.104$ roughly corresponds to the first cavity modal frequency where the cavity length is half a wavelength. This will cause a strong response of the plate at the first mode. Because the cross-modal effect is ignored here, the resonance points in Fig. 5 may not exactly match the absorption peaks in Fig. 3(c). Nevertheless, perforations on the plate play an important role of sound absorptions in the system resonance while the plate without perforations is only effective in reflecting sound at the first two modes. Therefore sound absorption at the resonance can compensate for the insufficiency of reflection in some frequency range for the plate with a weaker bending stiffness.

J. Acoust. Soc. Am., Vol. 132, No. 6, December 2012

Wang *et al.*: Hybrid silencer in a duct   3783
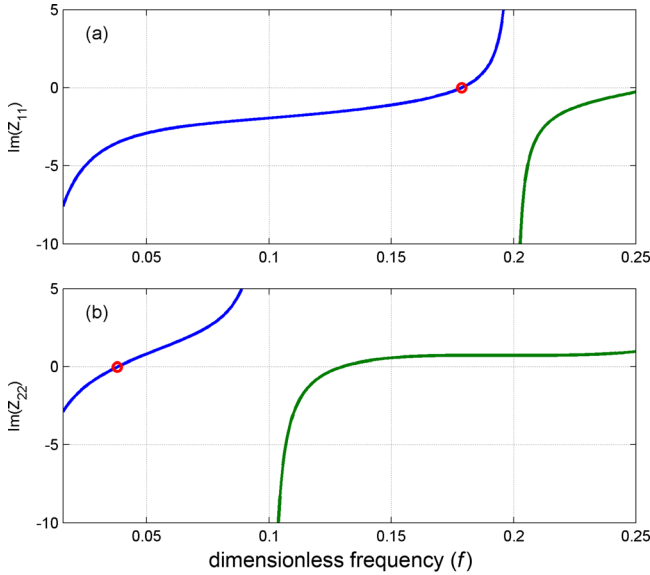
FIG. 5. (Color online) Total reactance of the first two modes. (a) $\text{Im}(Z_{11})$ and (b) $\text{Im}(Z_{22})$ for which the zero reactance is marked by an open circle.

E. Structural impedance

Without perforation, the dynamics of the plate with vibroacoustic coupling and the excitation force I_j can be described as follows:[2]

$$\{L_j + Z_{\text{duct},jl} - Z_{\text{cav},jl}\}V_{p,j} = -I_j. \qquad (32)$$

In order to investigate the effect of the perforation on the structural property, Eq. (23) is re-arranged into the following form:

$$\left\{\frac{L_j}{1-\sigma}\left(1 - \frac{\bar{V}_{0,j}}{V_{p,j}}\right) + (Z_{\text{duct},jl} - Z_{\text{cav},jl})\right\}\bar{V}_j = -I_j, \qquad (33)$$

where $\bar{V}_j = (1-\sigma)V_{p,j} + \bar{V}_{0,j}$ represents the smeared-out plate modal response including the average air velocity at the holes and that of the solid part of the plate. Comparing Eqs. (32) and (33) and keeping the same $Z_{\text{duct},jl}$ and $Z_{\text{cav},jl}$, an equivalent structure impedance of the plate with perforation $Z_{\text{struc\_eq},j}$ can be identified as

$$Z_{\text{struct\_eq},j} = \frac{L_j}{1-\sigma}\left(1 - \frac{\bar{V}_{0,j}}{V_{p,j}}\right). \qquad (34)$$

It is clear that, apart from the mass and bending stiffness of the structure itself, $Z_{\text{struc\_eq},j}$ is also affected by the velocity of the air motion of the perforation with respect to that of the plate. Figure 6 shows the resistant part [Figs. 6(1a) and 6(2a)], and the reactant part [Figs. 6(1b) and 6(2b)], of $Z_{\text{struct\_eq},1}$ and $Z_{\text{struct\_eq},2}$, with $B = 0.057$ and $m = 1$. Without perforation (dashed line), there is no resistance on the plate. Micro-perforations give raise to a resistive term for both the first and second mode, thus introducing damping on the plate. As shown in Figs. 6(2a) and 6(2b), the reactance curve appears to slightly shift to higher frequencies and the system becomes less massive for the frequency $f > 0.05$ for the first mode and $f > 0.09$ for the second mode, respectively. This can be regarded as a virtual negative mass effect brought up by the micro-perforation. Due to the decrease in the effective mass in the structural impedance at the second mode, the resonance of the system is shifted to a higher frequency. This is the reason why the modal reflection $|\bar{V}_jR_j|$ and the reflection coefficient β curves are shifted to higher frequencies when
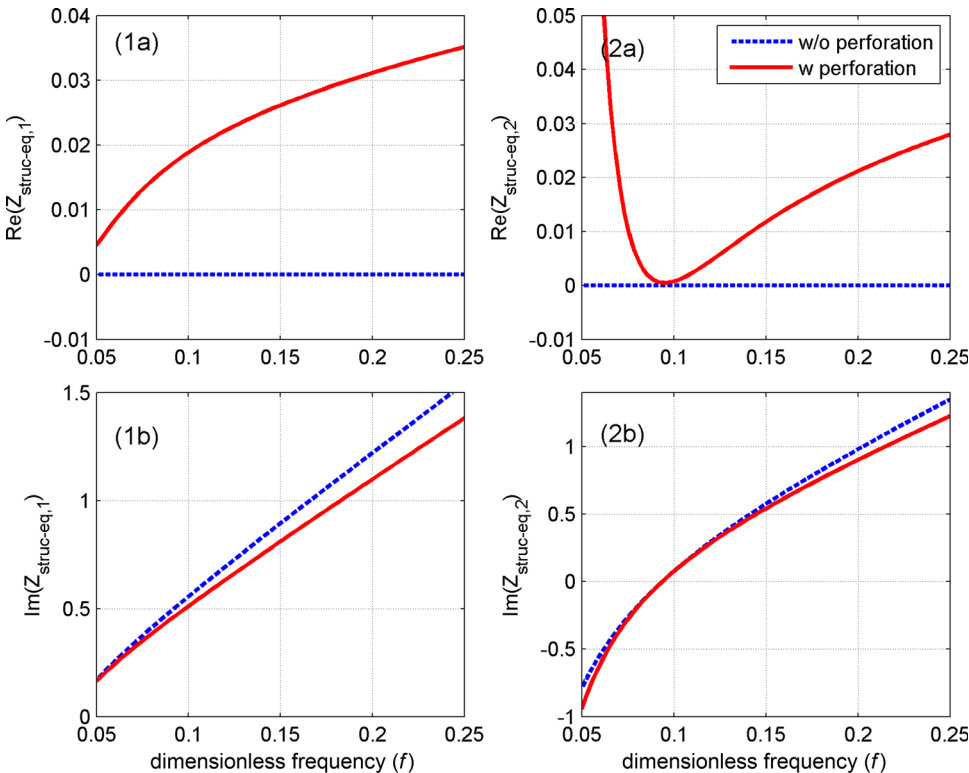
FIG. 6. (Color online) Equivalent structural impedance $Z_{\text{struc\_eq},j}$ for the first two modes, $j = 1, 2$. (1a) The resistant part of the first mode; (1b) reactant part of the first mode, (2a) resistant part of the second mode; and (2b) reactant part of the second mode.
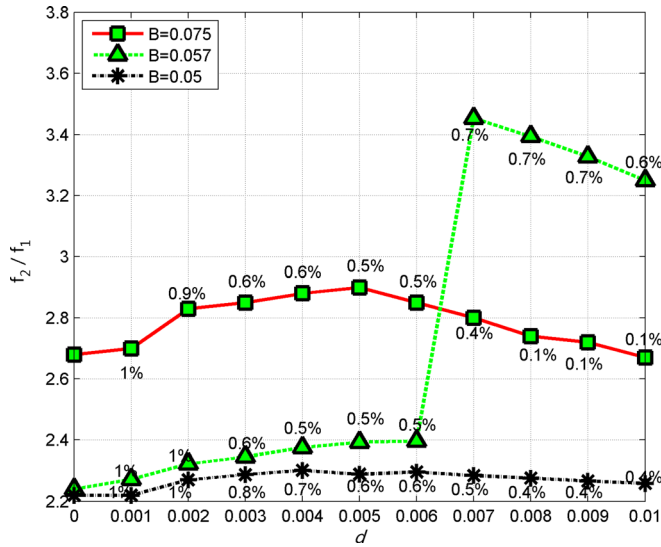
FIG. 7. (Color online) Optimization curve for different bending stiffness. The percentage on each point shows the perforation ratio to achieve the optimal f_2/f_1 with a corresponding diameter.

micro-perforation is added. Such a high frequency shift results in a higher band limit f_2, and subsequently the widening of the stopband.

F. Optimization of TL performance

The resistance and reactance of the micro-perforation are controlled by parameters such as the hole diameters and perforation ratio. They in turn affect the coupled system impedance, sound reflection, sound absorption, and ultimately the TL performance. Therefore, optimizations for parameters of a micro-perforated plate are necessary to achieve the best performance of the hybrid silencer. Figure 7 depicts the variation of bandwidth f_2/f_1 as a function of the optimal diameter

of the holes and perforation ratio for different bending stiffness. Three curves represent the search results for an optimal bandwidth with three typical bending stiffnesses. For the plate with a relatively weak bending stiffness $B = 0.05$ (dashed line with stars), the corresponding stopband remains at around $f_2/f_1 = 2.22$ with a very slight dependence on the hole size and perforation ratios. This is because the trough points between the second and third peak in TL spectrum (not shown here) are at a very low level and consequently the addition of micro-perforation does not lead to any significant increase in the TL at the trough point. For a very high bending stiffness $B = 0.075$ (solid line with squares), without perforation, the optimal stopband is relatively wide $f_2/f_1 = 2.68$. When the micro-perforation is added, the stopband remains in the range of 2.7 to 2.9. This means that the high bending stiffness of the plate itself can support the strong sound reflection. This effect alone can already substantiate a relatively broad stopband. The relative velocity of the holes and perforated plates cannot significantly influence the structural impedance due to the dominance by such a high bending stiffness. Therefore there is no tremendous change of the stopband when micro-perforation is introduced on the plate. The significance of the micro-perforation can be best seen when the bending stiffness of the plate falls into the intermediate range. With $B = 0.057$ (dashed line with triangles), excessive small perforation holes ($d < 0.006$) cannot significantly enlarge the stopband (typically ranging from $f_2/f_1 = 2.2$ to 2.4). On the other hand, when the size of the hole is further increased to $d = 0.007$ with the optimal perforation ratio $\sigma = 0.7\%$, the stopband is drastically increased to $f_2/f_1 = 3.45$. One can see an obvious change of the stopband for the hole size varying from $d = 0.006$ to $d = 0.007$ with proper selection of the perforation ratio. The above analyses seem to suggest that in order for the micro-perforation to take a dominant effect in enlarging the stopband of the
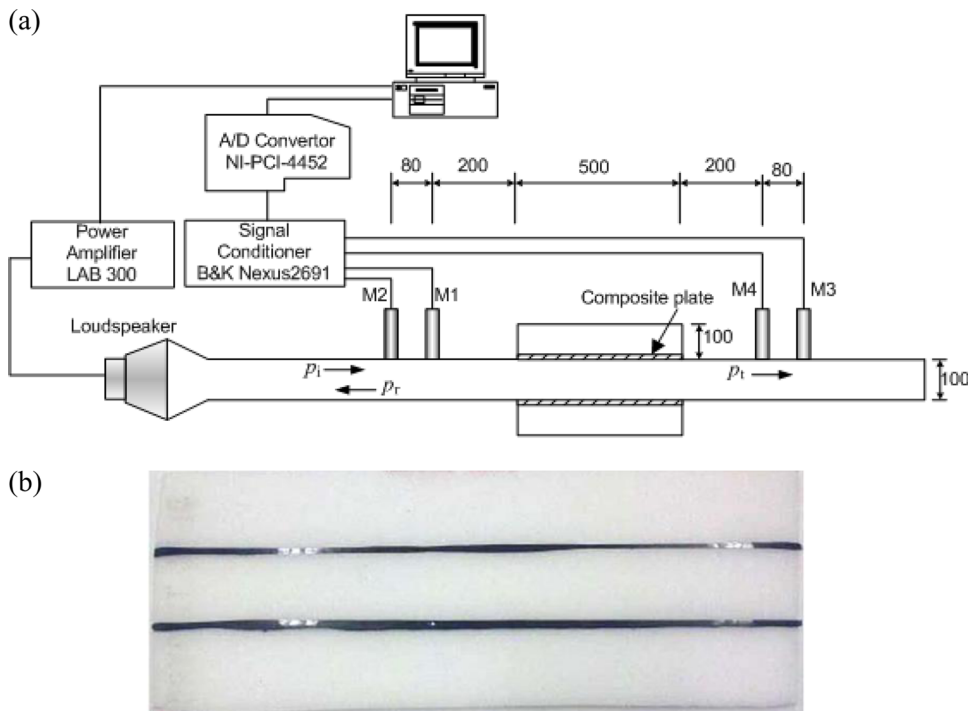
FIG. 8. (Color online) (a) Experimental set-up for TL measurement. (b) PMI reinforced by a CF.

J. Acoust. Soc. Am., Vol. 132, No. 6, December 2012

Wang *et al.*: Hybrid silencer in a duct   3785

hybrid silencer, a minimum level of bending stiffness of the plate is required. This will ensure a minimum of sound reflection in some frequency regions, while deficient ones will be taken care of by the sound micro-perforation. When properly designed, this hybrid silencer can provide a stopband which is even larger than a conventional plate silencer with a much higher stiffness as shown in Fig. 7. This is also a testimony of the hybrid nature of the proposed silencer, for which both reflection and absorption need to achieve a balance to bring out the hybrid effect.

IV. EXPERIMENTAL VALIDATION

An experiment was conducted to confirm the tendency predicted by the theoretical model. The TLs of the prototyped clamped plate with and without micro-perforations were measured and compared. The TL was measured by the four-microphone, two-load method.[21] As shown in Fig. 8(a), the incident noise is generated by a loudspeaker. Two pairs of 1/2 in., phase-matched microphones (B&K 4187) (Brüel & Kjær, Denmark) connected with a conditioning amplifier (B&K Nexus 2691) were used. The separation distance between the microphones was 80 mm. Signals from the microphones were acquired through an AD converter (NI-PCI-4452) (National Instruments). Both A/D and D/A processes were controlled by an NI LABVIEW program and were run by a loop of discrete frequency generation from 50 to 1000 Hz. By using two independent different downstream loading conditions to simulate the physical anechoic termination, the TL of the tested silencer was determined. The cross section of the duct was 100 mm × 100 mm and the corresponding cut-on frequency of the duct was about 1700 Hz. The two cavities also had a cross section of 100 mm × 100 mm and the length of 500 mm. Two pieces of composite plates which were made of polymethacrylimide (PMI) with the reinforcement of CF tows were installed flush with the duct.[3] The plate was 520 mm long, 104 mm wide, and 4 mm thick. The leading and trailing edges of the plates are clamped and the effective length of the plates was 500 mm. The two lateral edges of the plates were inserted into a thin gap between two constituent plates of the cavity walls. There was a very small clearance between the lateral edges of the plates and cavity wall such that the lateral edges could freely vibrate to simulate the two-dimensional behavior.

Figure 8(b) shows a photo of the configuration of the PMI foam plate reinforced with CF. The use of PMI is to reduce the mass of the plate while achieving the desired stiff-
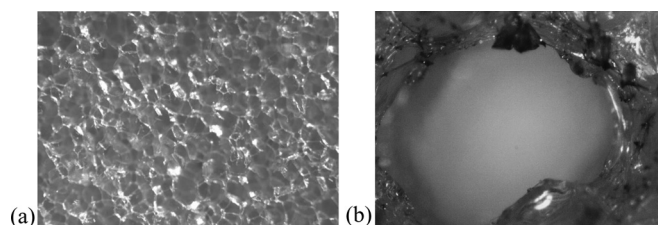
FIG. 9. The microscopic image of (a) a PMI foam plate and (b) one typical drilled hole with an irregular shape.
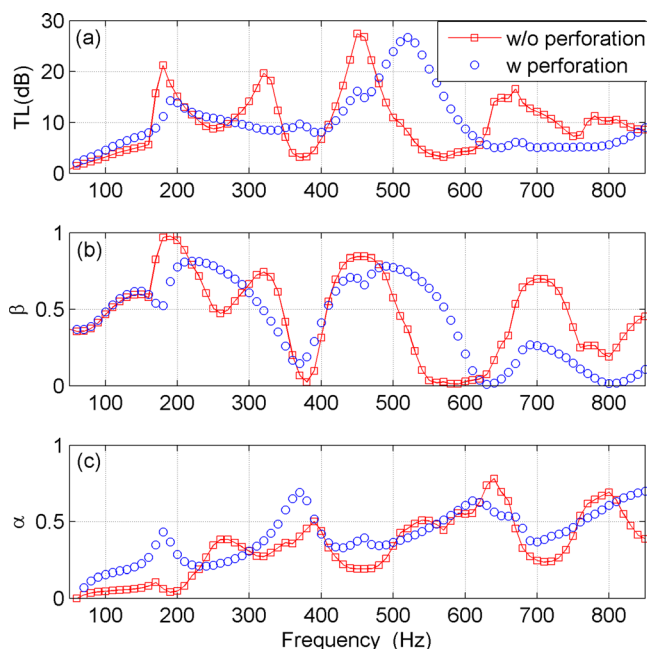
FIG. 10. (Color online) Comparison of experimental result of the plate ($m = 1$, $B = 0.057$, and $t = 4$ mm) without micro-perforations and that with micro-perforation of $d = 0.4$ mm and $\sigma = 0.5\%$ for the plate silencer. (a) TL, (b) reflection coefficient, and (c) absorption coefficient.

ness. As a type of porous material, seen in Fig. 9(a), however, the manufacturing process of drilling micro-perforated holes by a laser machine turned out to be very tedious and difficult to control the exact size of each hole as well as its shape. One typical drilled micro-perforated hole is shown in Fig. 9(b), illustrating the irregular shape of the hole. A close examination of the hole typology using a microscope revealed that the range of the drilled-hole diameter varied from 0.2 to 0.9 mm by using the laser drilling on this type of material, while the expected hole diameter is 0.4 mm. Therefore the intention here is not to validate the accuracy of the theoretical prediction. Instead, we would rather focus on confirming the micro-perforation effect predicted in the above analyses.

Figure 10 shows the measured TL of the plate with $B = 0.057$ (dimensional $B^* = 8.07$ kg·m²/s²) without perforations and that with perforations of $\sigma = 0.5\%$ and a hole size of 0.4 mm. Roughly speaking, the measured TL of the plate without perforations agrees quite well with the tendency predicted by the theoretical prediction shown in Fig. 2 (dashed line). There are two peaks in the stopband (TL > 10 dB). The measured TL for the plate with perforations also shows that the trough point at the frequency range from 350 to 400 Hz is raised up and the third peak is shifted to a higher frequency so that the band limit f_2 is extended from 500 to 590 Hz. Such an improvement is roughly in agreement with the theoretical predictions.

V. CONCLUSIONS

The performance of the plate silencer with micro-perforations has been investigated theoretically and experimentally. The benefit given by this hybrid plate silencer with the combination of sound reflection and absorption

mechanism is a more uniform TL spectrum with a wider stopband and a relaxation of the harsh requirement on the material property imposed by previous plate silencers. The following specific conclusions are drawn:

(1) A theoretical model, capable of dealing with the strong coupling between the vibrating micro-perforated plate and sound fields inside the cavity and the duct, is developed. The model is shown to be able to well characterize the hybrid behavior of the proposed silencer and therefore can be used as a useful design, analysis, and optimization tool.

(2) The theoretical study reveals that the proposed silencer in the form of a rectangular shape with two plates with micro-perforations can work effectively over a wide bandwidth. The stopband over 10 dB with the ratio $f_2/f_1 = 3.45$ can be achieved when the plate has a unit mass ratio and dimensionless bending stiffness of 0.057 with a micro-perforation hole size of $d = 0.007$ and a perforation ratio of 0.7%.

(3) The effects of the micro-perforations are threefold: (a) Micro-perforation introduces absorptions to the system. By doing so, the original TL trough point between the second and third peaks due to the insufficient sound reflection of the plate with a weaker bending stiffness can be lifted up, contributing to a broadening of the stopband. (b) Micro-perforation allows reducing the reactance of the equivalent structural impedance like a virtual negative mass. This results in a shift of the system resonance to higher frequencies, adding its contribution to the stopband broadening. (c) Along with the micro-perforation, the sound radiation and structural response of the plate is compromised through a dual process of pressure balance between the two sides of the plate and impaired sound radiation efficiency of the perforated plate. As a result, the sharp peaks on the TL curve provided by the original plate silencers are smoothed out. Altogether with the effects mentioned in (a) and (b), a more flattened/uniformed broadband silencer can be achieved.

(4) Optimization of the hybrid silencer is possible and becomes necessary for plates with a moderately high bending stiffness. The micro-perforation effect can be best seen when a minimum level of bending stiffness of the plate is ensured to substantiate a reasonable level of sound radiation. When properly designed, the hybrid silencer can provide a stopband which is even larger than a conventional plate silencer with a much higher stiffness.

(5) The micro-perforation effect revealed by theoretical and numerical analyses are confirmed by experiments.

[1] C. Q. Wang, J. Han, and L. X. Huang, "Optimization of a clamped plate silencer," J. Acoust. Soc. Am. **121**(2), 949–960 (2006).

[2] C. Q. Wang, L. Cheng, and L. X. Huang, "Realization of a broadband low-frequency plate silencer using sandwich plates," J. Sound Vib. **318**, 792–808 (2008).

[3] Y. S. Choy, Y. Liu, H. Y. Cheung, Q. Xi, and K. T. Lau, "Development of composite plate for compact silencer design," J. Sound Vib. **331**, 2348–2364 (2012).

[4] D. Y. Maa, "Potential of microperforated panel absorber," J. Acoust. Soc. Am. **104**(5), 2861–2866 (1998).

[5] H. V. Fuchs and X. Zha, "Acrylic-glass sound absorbers in the plenum of the Deutscher Bundestag," Appl. Acoust. **51**, 211–217 (1997).

[6] J. Kang and H. V. Fuchs, "Predicting the absorption of open weave textiles and microperforated membranes backed by an air space," J. Sound Vib. **220**, 905–920 (1999).

[7] H. Droltleff and X. Zhou, "Attractive room acoustic design for multi-purpose halls," Acta. Acust. **87**, 500–504 (2001).

[8] F. Asdrubali and G. Pispola, "Properties of transparent sound-absorbing panels for use in noise barriers," J. Acoust. Soc. Am. **121**, 214–221 (2007).

[9] M. Q. Wu, "Micro-perforated panels for duct silencing," Noise Control Eng. J. **45**, 69–77 (1997).

[10] Y. Guo, S. Allam, and M. Åbom, "Micro-perforated plate for vehicle applications," in *Proceedings of the 2008 Congress and Exposition of Noise Control Engineering, Inter-Noise 2008*, Shanghai, China (October 26–29, 2008).

[11] M. C. Chiu and Y. C. Chang, "Numerical studies on venting system with multi-chamber perforated mufflers by GA optimization," Appl. Acoust. **69**, 1017–1037 (2008).

[12] N. S. Dickey, A. Selamet, and J. M. Novak, "Multi-pass perforated tube silencers: A computational approach," J. Sound Vib. **211**(3), 435–448 (1998).

[13] Y. Y. Lee, E. W. M. Lee, and C. F. Ng, "Sound absorption of a finite flexible micro-perforated panel backed by an air cavity," J. Sound Vib. **287**, 227–243 (2005).

[14] C. Q. Wang, L. Cheng, J. Pan, and G. H. Yu, "Sound absorption of a micro-perforated panel backed by an irregular-shaped cavity," J. Acoust. Soc. Am. **127**(1), 238–246 (2010).

[15] L. Maxit, C. Yang, L. Cheng, and J. L. Guyader, "Modeling of micro-perforated panels in a complex vibro-acoustic environment using patch transfer function approach," J. Acoust. Soc. Am. **131**(3), 2118–2130 (2012).

[16] D. Takahashi and M. Tanaka, "Flexural vibration of perforated plated and porous elastic materials under acoustic loading," J. Acoust. Soc. Am. **112**(4), 1456–1464 (2002).

[17] P. E. Doak, "Excitation, transmission and radiation of sound from source distributions in hard-walled ducts of finite length (I): The effects of duct cross-section geometry and source distribution space-time pattern," J. Sound Vib. **31**, 1–72 (1973).

[18] L. Cheng, Y. Y. Li, and J. X. Gao, "Energy transmission in a mechanically-linked double-wall structure coupled to an acoustic enclosure," J. Acoust. Soc. Am. **117**(5), 2742–2751 (2005).

[19] F. Fahy and P. Gardonio, *Sound and Structural Vibration Radiation, Transmission and Response*. 2nd ed. (Academic Press, Burlington, MA, 2007), Chap. 3, pp. 157–159.

[20] A. Putra and D. J. Thompson, "Sound radiation from perforated plates," J. Sound Vib. **329**, 4227–4250 (2010).

[21] Y. S. Choy and L. X. Huang, "Experimental studies of a drumlike silencer," J. Acoust. Soc. Am. **112**(5), 2026–2035 (2002).